FINITE DEFORMATION THIN SHELL ANALYSIS FROM SCATTERED POINTS WITH MAXIMUM-ENTROPY APPROXIMANTS

Daniel Millán, Adrian Rosolen and Marino Arroyo

Laboratori de Càlcul Numèric (LaCàN), Departament de Matemàtica Aplicada III (MA3), Universitat Politècnica de Catalunya (UPC), Campus Nord UPC-C2, E-08034 Barcelona, Spain
marino.arroyo@upc.edu, http://www-lacan.upc.edu

Keywords: point-set surfaces, meshfree, *maximum-entropy* approximants, thin shells, finite deformations, nonlinear dimension reduction.

Abstract. We present a method to process embedded smooth surfaces using sets of points alone. The goal is to perform calculations on general point-set surfaces avoiding any global parameterization. We achieve this aim by approximating the point-set surface as an overlapping set of smooth local parametric descriptions. We combine three ingredients: (1) the automatic detection of the nonlinear local geometric structure of the surface by statistical learning methods, (2) the local parameterization of the surface using smooth meshfree (here *maximum-entropy*) approximants, and (3) patching together the local representations by means of a partition of unity.

Mesh-based methods can deal with surfaces of complex topology, since they rely on the element-level parameterizations, but cannot handle high-dimensional manifolds, whereas previous meshfree methods for thin shells consider a global parametric domain, which seriously limits the kinds of surfaces that can be treated.

We present the implementation of the method in the context of Kirchhoff-Love shells, but it is applicable to other calculations on manifolds in any dimension. With the smooth *maximum-entropy* approximants, this fourth-order partial differential equation is treated directly. We exemplify the flexibility of the proposed approach dealing with large deformations and surfaces of complex geometry.

1   INTRODUCTION

Over the last years, there has been a growing interest in the computer graphics community on point-based surface processing, which presents attractive features as compared to conventional mesh-based processing (Alexa et al., 2001; Pauly, 2003). In mesh-based methods, the mesh serves two useful purposes: it describes the geometry of the surface, and the elements provide local parametric spaces where the shape functions and the local parameterizations of the surface can be defined, and where the required calculations on the surface can be performed, e.g. for thin shell analysis. In these methods, the mesh generation can be difficult, they are not natural for point-based data, and they seem unpractical for embedded manifolds in high dimensional spaces. On the other hand, in the absence of a mesh, the notion of a surface defined from a set of scattered nodes becomes difficult to grasp. In particular, as noted in Levin (2003), a fundamental difficulty in defining basis functions and performing calculations on an embedded surface, as compared to open sets in Euclidean space, is the absence in general of a single parametric domain. Note carefully that in meshfree analysis, the basis functions are generally defined in physical space, which serves as parametric space as well.

In the computer graphics literature, Levoy and Whitted (1985) pioneered using points as primitives for geometric modeling and rendering of surfaces. Existing methods for describing a surface from a set of scattered points are generally based on implicit representations of the surface (Hoppe et al., 1992; Ohtake et al., 2003). Moving Least Squares (MLS) surfaces are a noteworthy example of point-based implicit surface representation, where the surface is defined as the set of fixed points of suitable projections (Levin, 2003, 1998). This idea has been very successful in the computer graphics community for rendering, either up or down sampling, and manipulating point-set models, see e.g. (Alexa et al., 2001; Pauly, 2003; Alexa et al., 2003; Amenta and Kil, 2004; Alexa et al., 2004). Despite the common themes and challenges, these developments have remained largely unconnected to the computational mechanics community. In this field, meshfree methods have been applied to thin-shell analysis, and the difficulty of defining an appropriate parametric space has been overcome by considering either a support mesh or very simple surfaces admitting a single parametric space (Krysl and Belytschko, 1996; Noguchi et al., 2000; Chen and Wang, 2006; Rabczuk et al., 2007).

Here, we extend the method proposed by Millan et al. (2010b) to perform numerical calculations on smooth manifolds described by scattered points. In our previous work, the method results from combining three ingredients. Firstly, the local geometric structure of the manifold is detected from the node set using weighted Principal Component Analysis (wPCA) which identifies the hyperplane closest to the points in a given neighborhood that we call patch. This plane is then used as the local parametric space to construct the meshfree maximum-entropy (*max-ent*) basis functions (Arroyo and Ortiz, 2006; Cyron et al., 2009) and the local smooth parameterization of the manifold. Secondly, the smooth parameterization in each patch can be realized with a variety of methods, from other mesh-free methods such as MLS approximants to mesh-based methods such as subdivision finite elements. In the latter case, no global mesh is required. Here the local *max-ent* approximants (Arroyo and Ortiz, 2006) are chosen, due to their smoothness, robustness, and relative ease of quadrature relative to other meshfree approximants. Finally, the different local parameterizations are then glued together with a Partition of Unity (PU) defined in the ambient space, which consequently is also a PU in the embedded manifold. Specifically, functionals defined on the surface are readily split into local contributions, each involving a single local parameterization. This method avoids any global parametric domain, required in previous meshfree methods, which greatly expands its range of applicabil-

ity. Even though we exercise here the method for surfaces in $\mathbb{R}^3$, it is applicable to perform calculations on embedded manifolds in any space dimension, unlike mesh-based methods.

In the present paper we make use of the novel nonlinear dimension reduction methodology Modified Local Linear Embedding (MLLE see Zhang and Wang (2007)) instead of wPCA. The advantage of nonlinear dimension reduction techniques is that they allow us to consider challenging point-set manifolds in an efficient and robust fashion.

The outline of the paper is as follows. Section 2 describes the proposed methodology for point-set manifold processing. Next, Section 3, provides a short account of the Kirchhoff–Love shell theory. Throughout the present work we confine our attention to the theory of shells under static loading. Numerical experiments to evaluate the capability of the method are presented in Section 4. Some remarks and conclusions are collected in Section 5.

2 MANIFOLD DESCRIPTION FROM SCATTERED POINTS

We consider a smooth $d-$manifold $\mathcal{M}$ embedded in $\mathbb{R}^D$, $d \leq D$. Our aim is to obtain a numerical representation of $\mathcal{M}$, and make computations on it.

Let $P = \{\boldsymbol{P}_1, \boldsymbol{P}_2, \ldots, \boldsymbol{P}_N\} \subset \mathbb{R}^D$ be a set of control points representing $\mathcal{M}$. We consider another set of geometric markers, $Q = \{\boldsymbol{Q}_1, \boldsymbol{Q}_2, \ldots, \boldsymbol{Q}_M\}$, typically a subset of P but not necessarily. For simplicity, we will denote the points in P and its associated objects with a lower case subindex, e.g. $\boldsymbol{P}_a$, for $a = 1, 2, \ldots, N$, and the geometric markers in Q and its associated objects with an upper case subindex, e.g. $\boldsymbol{Q}_A$, for $A = 1, 2, \ldots, M$.

We partition these geometric markers into L groups on the basis of proximity (Metis domain decomposition with a k-NN graph). We represent these groups of geometric markers with index sets $\mathcal{I}_\kappa, \kappa = 1, \cdots, L$ with $\cup_{\kappa=1}^{L} \mathcal{I}_\kappa = \{1, 2, \ldots, M\}$ and $\mathcal{I}_\kappa \cap \mathcal{I}_\iota = \emptyset$, and use Greek subindices to refer to entities associated with these groups of markers. As it will become clear below, there is a one-to-one correspondence between these groups of geometric markers and the local parameterizations of the surface, which we call patches.

We consider a Shepard partition of unity associated with the geometric markers. Consider a set of non-negative reals $\{\beta_A\}_{A=1,2,\ldots,M}$ associated with each point in Q. We define the Shepard partition of unity with Gaussian weight associated to the set Q as the functions $w_A : \mathbb{R}^D \to \mathbb{R}$ for $A = 1, 2, \ldots, M$ given by

$$w_A(\boldsymbol{x}) = \frac{\exp(-\beta_A |\boldsymbol{x} - \boldsymbol{Q}_A|^2)}{\sum_{B=1}^{M} \exp(-\beta_B |\boldsymbol{x} - \boldsymbol{Q}_B|^2)}. \tag{1}$$

For efficiency, and given the fast decay of the Gaussian functions, these functions are numerically treated as compactly supported.

We aggregate these partition of unity functions by patches, yielding a coarser set of partition of unity functions

$$\psi_\kappa(\boldsymbol{x}) = \sum_{A \in \mathcal{I}_\kappa} w_A(\boldsymbol{x}). \tag{2}$$

These functions form a partition of unity in $\mathbb{R}^D$, and consequently also in $\mathcal{M}$. We finally consider the index sets of all control points influencing each patch, $\mathcal{J}_\kappa$, with $\cup_{\kappa=1}^{L} \mathcal{J}_\kappa = \{1, 2, \ldots, N\}$, but now $\mathcal{J}_\kappa \cap \mathcal{J}_\iota \neq \emptyset$ to provide overlap between the local descriptions. Roughly speaking, these sets are $\{a \mid \boldsymbol{P}_a \in \sup \psi_\kappa\}$, slightly enlarged so that the patch parameterization is smooth on the boundary of the support of ψ_κ.

2.1   Local manifold learning

We process the points $P_\kappa = \{\boldsymbol{P}_a\}_{a \in \mathcal{J}_\kappa}$ with MLLE. The outcome is a nonlinear model reduction mapping

$$
\begin{aligned}
R_\kappa : P_\kappa &\longrightarrow \mathbb{R}^d \\
\boldsymbol{P}_a &\longmapsto \boldsymbol{\xi}_a
\end{aligned}
\tag{3}
$$

The reduced node set $\Xi_\kappa = \{\boldsymbol{\xi}_a\}_{a \in \mathcal{J}_\kappa} \in \mathbb{R}^d$ captures the right dimensionality and local geometry of the original set of points, even if these lie on a curved manifold, provided the manifold is sufficiently sampled. This mapping tries to be as isometric as possible. If metric distortions are too large, then the partitions can be made smaller.

2.2   Local parameterization

The outcome of R_κ provides a convenient parametric space for the embedded manifold. Suppose we have smooth approximants $p_a(\boldsymbol{\xi})$ associated to the point set Ξ_κ on a subset $\mathscr{A}_\kappa$ of $\mathbb{R}^d$, here the convex hull of the reduced node set $\operatorname{conv} \Xi_\kappa$. We locally parameterize the manifold in this patch as

$$
\begin{aligned}
\boldsymbol{\varphi}_\kappa : \mathbb{R}^d \supset \operatorname{conv} \Xi_\kappa &\longrightarrow \mathbb{R}^D \\
\boldsymbol{\xi} &\longmapsto \sum_{a \in \mathcal{J}_\kappa} p_a(\boldsymbol{\xi})\, \boldsymbol{P}_a
\end{aligned}
\tag{4}
$$

The image of $\mathscr{A}_\kappa = \operatorname{conv} \Xi_\kappa$ through the parameterization $\boldsymbol{\varphi}_\kappa$, $\mathcal{M}_\kappa$, is a local approximation of the manifold.

2.3   Partition of unity to evaluate integrals on $\mathcal{M}$

A partition of unity is a classical technique to patch together local constructions on a manifold do Carmo (1976). Consider now the integral of a scalar function f over a manifold $\mathcal{M}$, $f : \mathcal{M} \to \mathbb{R}$. This function can also depend on other fields, as in a functional over the manifold or its associated weak form. Then we have the following identity

$$
\int_\mathcal{M} f(\boldsymbol{x})\, d\mathcal{M} = \sum_{\kappa=1}^L \int_\mathcal{M} \psi_\kappa(\boldsymbol{x})\, f(\boldsymbol{x})\, d\mathcal{M}.
\tag{5}
$$

Combining the partition of unity with the local parameterization of the κ-th patch. we can approximate numerically integrals over the manifold $\mathcal{M}$ described by a set of scattered points as

$$
\int_\mathcal{M} f(\boldsymbol{x})\, d\mathcal{M} \simeq \sum_{\kappa=1}^L \int_{\mathscr{A}_\kappa} \psi_\kappa(\boldsymbol{\varphi}_\kappa(\boldsymbol{\xi}))\, f(\boldsymbol{\varphi}_\kappa(\boldsymbol{\xi}))\, J_\kappa(\boldsymbol{\xi})\, d\boldsymbol{\xi}
\tag{6}
$$

where $\mathscr{A}_\kappa$ is the parametric space associated to the κ−th patch, and $J_\kappa = \sqrt{\det\left[(D\boldsymbol{\varphi}_\kappa)^T D\boldsymbol{\varphi}_\kappa\right]}$ is the Jacobian determinant of the parameterization. In this way, similarly to finite element methods, we have split the integral into local contributions which can be evaluated using local parameterizations.

The last integral can be subsequently approximated by numerical quadrature on the local parametric space. Here, we use Gauss quadrature on a support triangulation defined over Ξ_κ. The integrand often does not depend explicitly on $\boldsymbol{x}$, and we express f in terms of $\boldsymbol{\xi}$ directly. This is not the case for the partition of unity functions, which are defined on the ambient space $\mathbb{R}^D$.

3 THIN-SHELL MODEL

In this section, we review the mechanics of thin shells (Cirak et al., 2000; Cirak and Ortiz, 2001), based on the geometrically exact formulation in Simo and Fox (1989); Simo et al. (1989). Here we restrict our attention to the Kirchhoff–Love theory of shells, i.e. we neglect the shearing and stretching deformation normal to the shell mid-surface. In this theory, the shell director remains normal to the mid-surface during the deformation.

We follow the usual convention for Latin and Greek indices (i.e. $i = 1, 2, 3$; $\alpha = 1, 2$), a comma denotes partial differentiation, subscripts refer to covariant components, and superscripts denote contravariant components.

3.1 Kinematics of the shell

We next describe the kinematics of a thin-shell body $\mathscr{S} \subset$ in three-space. We assume that this body can be described by the pair $(\boldsymbol{\varphi}, \boldsymbol{t})$, where the mapping $\boldsymbol{\varphi}$ defines the shell middle surface, Ω, and $\boldsymbol{t}$ is a field of unit vectors (a field of directors). We assume the thickness h of the shell to be uniform for simplicity, and also we assume that the change in shell thickness after deformation is negligible. Then, the thin shell body $\mathscr{S}$ is given by

$$\mathscr{S} = \left\{ \boldsymbol{x} \in \mathbb{R}^3 \mid \boldsymbol{x} = \boldsymbol{\varphi}(\xi^\alpha) + \xi \, \boldsymbol{t}(\xi^\alpha), \ -\frac{h}{2} \leq \xi \leq \frac{h}{2}, \ (\xi^1, \xi^2) \in \mathscr{A} \right\}, \tag{7}$$

where $\mathscr{A} \subset \mathbb{R}^2$ is the parametric space for the middle surface. Hence, we view a configuration $\boldsymbol{x}$ as a mapping from a parametric domain $\mathscr{A} \times [-h/2, h/2]$ into $\mathbb{R}^3$. The parametric domain is described by the coordinates $\{\xi^1, \xi^2, \xi^3\}$ (where we identify $\xi = \xi^3$), whose corresponding dual basis is $\{\boldsymbol{E}^i\}$. The area element of the middle surface can be computed as $d\Omega = \bar{j} \, d\xi^1 d\xi^2$, where $\bar{j} = \left\| \boldsymbol{\varphi}_{,1} \times \boldsymbol{\varphi}_{,2} \right\|$. The tangent map of a given configuration $T\boldsymbol{x}$ can be computed from the convective basis vectors $\boldsymbol{g}_i$ as

$$T\boldsymbol{x} = \frac{\partial \boldsymbol{x}}{\partial \xi^i} \otimes \boldsymbol{E}^i = \boldsymbol{g}_i \otimes \boldsymbol{E}^i,$$

with $\boldsymbol{g}_\alpha = \frac{\partial \boldsymbol{x}}{\partial \xi^\alpha} = \boldsymbol{\varphi}_{,\alpha} + \xi \, \boldsymbol{t}_{,\alpha}$ and $\boldsymbol{g}_3 = \frac{\partial \boldsymbol{x}}{\partial \xi} = \boldsymbol{t}$. The covariant components of the metric tensor in convected coordinates are given by $g_{ij} = \boldsymbol{g}_i \cdot \boldsymbol{g}_j$.

Hereinafter, subscript 0 denotes quantities in the reference configuration, for instance $\boldsymbol{\varphi}_0$ is a point on the reference middle surface. A deformation mapping is a mapping from a reference body into $\mathbb{R}^3$, $\boldsymbol{x} \circ \boldsymbol{x}_0^{-1}$. Consequently, the deformation gradient is $\boldsymbol{F} = T\boldsymbol{x} \, (T\boldsymbol{x}_0)^{-1}$, and the Jacobian is $J = \det(\boldsymbol{F}) = j/j_0$, where $j = \det(T\boldsymbol{x}) = \boldsymbol{g}_3 \cdot (\boldsymbol{g}_1 \times \boldsymbol{g}_2)$.

The shell director in the reference configuration $\boldsymbol{t}_0$ coincides with the normal to the undeformed middle surface of the shell and hence has the properties

$$\boldsymbol{t}_0 = \frac{\boldsymbol{\varphi}_{0,1} \times \boldsymbol{\varphi}_{0,2}}{\bar{j}_0}, \quad \boldsymbol{\varphi}_{0,\alpha} \cdot \boldsymbol{t}_0 = 0, \quad |\boldsymbol{t}_0| = 1, \quad \boldsymbol{t}_0 \cdot \boldsymbol{t}_{0,\alpha} = 0.$$

In general, the director in the deformed configuration of the shell, $\boldsymbol{t}$, is allowed to be an arbitrary vector field over $\Omega = \boldsymbol{x}(\mathscr{A} \times \{0\})$.

The local shell deformations can be characterized by the Green–Lagrange strain tensor. Since the convected components of the metric tensor coincide with the components of $(T\boldsymbol{x})^T T\boldsymbol{x}$ in the basis associated with $\{\xi^i\}$, the Green–Lagrange strain tensor can be expressed as the difference between the metric tensors on the deformed and undeformed configurations of the shell, i.e.

$$E_{ij} = \frac{1}{2} \left(g_{ij} - g_{0ij} \right) = \frac{1}{2} (\boldsymbol{x}_{,i} \cdot \boldsymbol{x}_{,j} - \boldsymbol{x}_{0,i} \cdot \boldsymbol{x}_{0,j}).$$

Plugging the basic kinematic ansatz $\boldsymbol{x} = \boldsymbol{\varphi}(\xi^\alpha) + \xi\,\boldsymbol{t}(\xi^\alpha)$ into the above expression, and grouping terms, we obtain

$$E_{ij} = \varepsilon_{ij} + \xi\,\rho_{ij} + (\xi)^2\,\vartheta_{ij}, \tag{8}$$

which admits the following interpretation in terms of the symmetric tensors ε_{ij}, ρ_{ij} and ϑ_{ij}:

- The membrane strain tensor $\varepsilon_{\alpha\beta} = \frac{1}{2}(\boldsymbol{\varphi}_{,\alpha} \cdot \boldsymbol{\varphi}_{,\beta} - \boldsymbol{\varphi}_{0,\alpha} \cdot \boldsymbol{\varphi}_{,\beta})$, which lives on the middle surface, measures the in-plane deformation of the surface; the components $\varepsilon_{\alpha3} = \frac{1}{2}\boldsymbol{\varphi}_{,\alpha} \cdot \boldsymbol{t}$ measure the shearing of the director $\boldsymbol{t}_0$; and the component $\varepsilon_{33} = \frac{1}{2}(\boldsymbol{t} \cdot \boldsymbol{t} - 1)$ measures the stretching of the director $\boldsymbol{t}_0$.

- The bending or change in curvature of the shell is measured by the tensor $\rho_{\alpha\beta} = \boldsymbol{\varphi}_{,\alpha} \cdot \boldsymbol{t}_{,\beta} - \boldsymbol{\varphi}_{0,\alpha} \cdot \boldsymbol{t}_{0,\beta}$, and $\rho_{\alpha3} = \frac{1}{2}\boldsymbol{t}_{,\alpha} \cdot \boldsymbol{t}$ measures the shearing originated from the director elongation; the in-plane tensor $\vartheta_{\alpha\beta} = \frac{1}{2}(\boldsymbol{t}_{,\alpha} \cdot \boldsymbol{t}_{,\beta} - \boldsymbol{t}_{0,\alpha} \cdot \boldsymbol{t}_{0,\beta})$ is exclusively related to changes of the middle surface directors. The rest of the components vanish, $\rho_{33} = \vartheta_{3i} = \vartheta_{i3} = 0$.

3.2 Kirchhoff–Love hypothesis

In the remainder of this section we restrict our attention to the Kirchhoff–Love theory of thin shells, i.e. we constrain the deformed director $\boldsymbol{t}$ to coincide with the unit normal of the deformed middle surface of the shell, i.e.

$$\boldsymbol{t} = \frac{\boldsymbol{\varphi}_{,1} \times \boldsymbol{\varphi}_{,2}}{\bar{j}}, \quad \boldsymbol{\varphi}_{,\alpha} \cdot \boldsymbol{t} = 0, \quad |\boldsymbol{t}| = 1, \quad \boldsymbol{t} \cdot \boldsymbol{t}_{,\alpha} = 0.$$

Consequently, the theory can be formulated exclusively in terms of the shell middle surface. We introduce its first and second fundamental forms expressed in convected components

$$a_{\alpha\beta} = \boldsymbol{\varphi}_{,\alpha} \cdot \boldsymbol{\varphi}_{,\beta},$$
$$\kappa_{\alpha\beta} = \boldsymbol{\varphi}_{,\alpha} \cdot \boldsymbol{t}_{,\beta} = -\boldsymbol{\varphi}_{,\alpha\beta} \cdot \boldsymbol{t}.$$

Here we have identified the director with the normal. With the Kirchhoff–Love hypothesis, the only remaining non-zero components of the Green–Lagrange strain tensor are

$$\begin{aligned} E_{\alpha\beta} &= \tfrac{1}{2}(a_{\alpha\beta} - a_{0\alpha\beta}) + \xi(\kappa_{\alpha\beta} - \kappa_{0\alpha\beta}) + \tfrac{(\xi)^2}{2}(\boldsymbol{t}_{,\alpha} \cdot \boldsymbol{t}_{,\beta} - \boldsymbol{t}_{0,\alpha} \cdot \boldsymbol{t}_{0,\beta}) \\ &= \varepsilon_{\alpha\beta} + \xi\,\rho_{\alpha\beta} + (\xi)^2\,\vartheta_{\alpha\beta}. \end{aligned} \tag{9}$$

3.3 Equilibrium configuration of thin shells

The potential energy of an elastic shell body with internal energy density W can be expressed in terms of the displacement $\boldsymbol{u} = \boldsymbol{\varphi} - \boldsymbol{\varphi}_0$ of a material point on the shell midsurface by the functional

$$\Pi[\boldsymbol{u}] = \int_{\mathscr{S}_0} W(\boldsymbol{u})\,dV_0 + \Pi_{\texttt{ext}}[\boldsymbol{u}],$$

where $\Pi_{\texttt{ext}}$ is the potential energy of the external loads. For concreteness, we consider an isotropic Kirchhoff–St. Venant elastic material, with an internal energy density expressed as (Ciarlet, 2000)

$$W = \frac{1}{2}C^{ijkl}E_{ij}E_{kl},$$

where C^{ijkl} are the contravariant components of the elasticity tensor.

For thin shell bodies, the Green-Lagrange tensor components are commonly retained up to first order in h, see Eq. (9), and the effect of curvature on the configuration Jacobian away

from the middle surface is neglected, that is $j_0/\bar{j}_0 = 1$ (see Simo and Fox (1989); Simo et al. (1989)). Assuming that the elasticity tensor does not vary trough the thickness, the internal energy density can be integrated through-the-thickness, resulting in an internal energy density per unit area

$$\mathcal{W} = \frac{1}{2} \int_{-h/2}^{h/2} C^{\alpha\beta\gamma\delta} E_{\alpha\beta} E_{\gamma\delta} \frac{j_0}{\bar{j}_0} \, d\xi \simeq \frac{1}{2} C^{\alpha\beta\gamma\delta} \left(h\varepsilon_{\alpha\beta}\varepsilon_{\gamma\delta} + \frac{h^3}{12} \rho_{\alpha\beta}\rho_{\gamma\delta} \right),$$

with

$$C^{\alpha\beta\gamma\delta} = \frac{E}{(1-\nu^2)} \left[\nu a_0^{\alpha\beta} a_0^{\gamma\delta} + \frac{1}{2}(1-\nu)\left(a_0^{\alpha\gamma} a_0^{\beta\delta} + a_0^{\alpha\delta} a_0^{\beta\gamma} \right) \right],$$

where $a_0^{\alpha\gamma}(a_0)_{\gamma\beta} = \delta_\beta^\alpha$, E is the Young's modulus, and ν the Poisson's ratio. Thus, the internal potential energy can be written as an integral over the reference middle surface

$$\Pi_{\texttt{int}}[\boldsymbol{u}] = \int_{\Omega_0} \mathcal{W}(\boldsymbol{u}) \, d\Omega_0,$$

and the external potential becomes

$$\Pi_{\texttt{ext}}[\boldsymbol{u}] = - \int_{\Omega_0} \boldsymbol{q} \cdot \boldsymbol{u} \, d\Omega_0 - \int_{\partial\Omega_0} \boldsymbol{h} \cdot \boldsymbol{u} \, d\ell_0,$$

where $\boldsymbol{q}$ is the external body load per unit area, $\boldsymbol{h}$ the forces per unit length applied on the boundary of the middle surface, and $d\ell_0$ is the line element of the boundary of the middle surface.

Following Simo and Fox (1989), we introduce the elastic constitutive relations between the shell stresses and the strains as

$$n^{\alpha\beta} = \frac{\partial\mathcal{W}}{\partial\varepsilon_{\alpha\beta}} = h\,C^{\alpha\beta\gamma\delta}\varepsilon_{\gamma\delta},$$
$$m^{\alpha\beta} = \frac{\partial\mathcal{W}}{\partial\rho_{\alpha\beta}} = \frac{h^3}{12}C^{\alpha\beta\gamma\delta}\rho_{\gamma\delta},$$

where $n^{\alpha\beta}$ is the effective membrane stress and $m^{\alpha\beta}$ is the effective bending stress, which can be interpreted as force and moment resultants. Further, by recourse to the Voigt's notation, we obtain the following convenient expressions

$$\boldsymbol{n} = \begin{pmatrix} n^{11} \\ n^{22} \\ n^{12} \end{pmatrix} = h\boldsymbol{C}\boldsymbol{\varepsilon}, \quad \boldsymbol{m} = \begin{pmatrix} m^{11} \\ m^{22} \\ m^{12} \end{pmatrix} = \frac{h^3}{12}\boldsymbol{C}\boldsymbol{\rho}, \quad \boldsymbol{\varepsilon} = \begin{pmatrix} \varepsilon_{11} \\ \varepsilon_{22} \\ 2\varepsilon_{12} \end{pmatrix}, \quad \boldsymbol{\rho} = \begin{pmatrix} \rho_{11} \\ \rho_{22} \\ 2\rho_{12} \end{pmatrix},$$

where the matrix $\boldsymbol{C}$ is given by the expression

$$\boldsymbol{C} = \frac{E}{1-\nu^2} \begin{pmatrix} (a_0^{11})^2 & \nu a_0^{11} a_0^{22} + (1-\nu)(a_0^{12})^2 & a_0^{11} a_0^{12} \\ & (a_0^{22})^2 & a_0^{22} a_0^{12} \\ symm & & \frac{1}{2}\left[(1-\nu)a_0^{11} a_0^{22} - (1+\nu)(a_0^{12})^2\right] \end{pmatrix}.$$

Finally, with the above definitions, we can write the principle of virtual work in terms of integrals over the parametric space $\mathscr{A}$ as follows

$$0 = \delta\Pi[\boldsymbol{u},\delta\boldsymbol{u}] = \int_{\mathscr{A}} (\delta\boldsymbol{\varepsilon} \cdot \boldsymbol{n} + \delta\boldsymbol{\rho} \cdot \boldsymbol{m}) \, \bar{j}_0 \, d\xi^1 d\xi^2 + \delta\Pi_{\texttt{ext}}[\delta\boldsymbol{u}]. \tag{10}$$

3.4   Galerkin discretization

We consider now the discrete equilibrium equations for surfaces numerically represented with the procedure described before, in terms of a set of nodes $P = \{\boldsymbol{P}_a\}$, $a = 1, ..., N$, and a set of L patches identified with the marker points $Q = \{\boldsymbol{Q}_A\}$, $A = 1, ..., M$.

Let $\boldsymbol{\varphi}_{0\kappa}$ be a configuration mapping for the middle surface from a specific patch κ, defined over the parametric space $\mathscr{A}_\kappa$

$$\boldsymbol{\varphi}_{0\kappa}(\boldsymbol{\xi}) = \sum_{a \in \mathcal{J}_\kappa} p_a(\boldsymbol{\xi}) \, \boldsymbol{P}_a, \tag{11}$$

as described in Section 2.2. We represent the displacement field in a given subdomain κ as

$$\boldsymbol{u}_\kappa(\boldsymbol{\xi}) = \sum_{a \in \mathcal{J}_\kappa} p_a(\boldsymbol{\xi}) \, \boldsymbol{u}_a. \tag{12}$$

Virtual displacements are represented likewise. With the strategy presented in Section 2.3, we can split the integrals in the principle of virtual work into patch contributions, e.g.

$$\delta\Pi[\boldsymbol{u}, \delta\boldsymbol{u}] = \sum_{\kappa=1}^{L} \int_{\mathscr{A}_\kappa} \left[(\delta\boldsymbol{\varepsilon} \cdot \boldsymbol{n} + \delta\boldsymbol{\rho} \cdot \boldsymbol{m}) \, \bar{j}_0 \right]_\kappa (\psi_\kappa \circ \boldsymbol{\varphi}_0) \, d\xi^1 d\xi^2 + \delta\Pi_{\texttt{ext}}[\delta\boldsymbol{u}]. \tag{13}$$

Here, $[\cdot]_\kappa$ means that the expression within the brackets is evaluated with the κ-th patch approximation of the undeformed middle surface, the displacement field, and the virtual displacement field.

Introduction of discretization from Eq. (12) into the weak form in Eq. (13) yields a semi-discrete system of equations of the form

$$\boldsymbol{f}_{int}^a = \boldsymbol{f}_{ext}^a, \tag{14}$$

where $\boldsymbol{f}_{int}^a$ and $\boldsymbol{f}_{ext}^a$ are the internal and external force array, respectively. Details about that expressions are indicated in the work of Millan et al. (2010a).

4   NUMERICAL EXAMPLES

4.1   Point indentation of a spherical cap

This numerical experiment mimics the simple experiment of indenting a plastic bottle (Vaziri and Mahadevan, 2008). It is modeled as a spherical shell cap subject to a concentrated apex load. When the deformation reaches a magnitude comparable to the shell thickness the response becomes nonlinear, and the deformed configuration moves through polyhedral shapes, starting in a triangle (see Fig. 1). Material have Young's modulus $E = 10^9$, and Poisson ratio $\nu = 0.3$, the thickness of the shell is $h = 0.005$.

4.2   Pullout of a bunny

This example illustrates the ability of the method to deal with shells of complex geometry, defined by a set of points alone, without the need for a global surface mesh. The quality of the node and marker sets should be sufficiently good and adapted to complex geometric features, here the ears. Material parameters have been selected as $E = 10^7$, and $\nu = 0.3$, while the thickness of the thin shell is $h = 0.005$. Fig. 2 shows a sketch of the classical Stanford bunny being pulled by a pair of forces, and also the deformed geometry is portrayed.
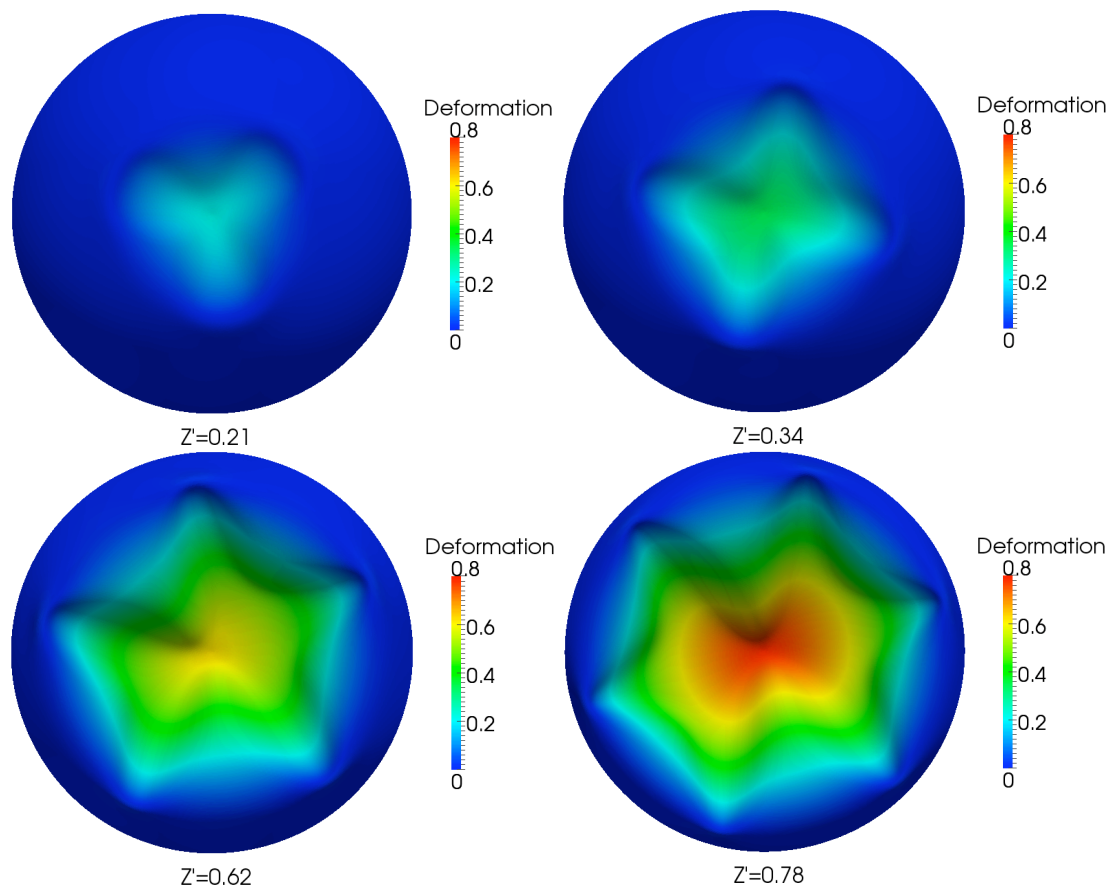
Figure 1: Page layout

5 CONCLUSIONS

We have extended the methodology proposed by Millan et al. (2010b) for processing d-dimensional point-set manifolds embedded in $\mathbb{R}^D$, which avoids a global parameterization or a mesh. We have developed a method that dramatically reduce the number of patches (i.e. the number of local parameterizations and partition of unity functions) relative to the number of nodes. With the previous method, which uses wPCA, the density of patches was limited by the geometric features of the surface, in that the projections should not distort too much the node geometry.

We have applied the method to the Kirchhoff-Love thin shell analysis. The proposed method significantly extends the applicability of meshfree methods to thin-shell analysis, in that it liberates such methods from the burden of requiring a single parametric space, or imposing cumbersome patching conditions between meshfree macro-elements. This feature is illustrated by an example of a shell of complex geometry.
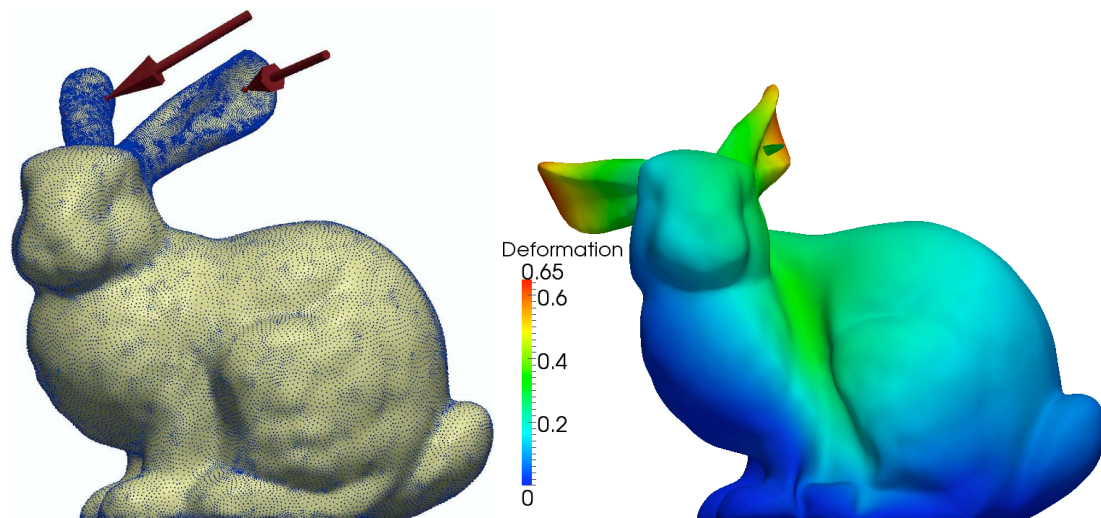
Figure 2: Page layout

REFERENCES

Alexa M., Behr J., Cohen-Or D., Fleishman S., Levin D., and Silva C. Point set surfaces. In *VIS '01: Proceedings of the conference on Visualization '01*, pages 21–28. IEEE Computer Society, Washington, DC, USA, 2001. ISBN 0-7803-7200-X.

Alexa M., Behr J., Cohen-Or D., Fleishman S., Levin D., and Silva C. Computing and rendering point set surfaces. *Transactions on Visualization and Computer Graphics*, 9(1):3–15, 2003.

Alexa M., Gross M., Pauly M., Pfister H., Stamminger M., and Zwicker M. Point-based computer graphics. SIGGRAPH 2004 Course Notes, 2004.

Amenta N. and Kil Y. Defining point-set surfaces. *ACM Transactions on Graphics*, 23(3):264–270, 2004. ISSN 0730-0301.

Arroyo M. and Ortiz M. Local maximum-entropy approximation schemes: a seamless bridge between finite elements and meshfree methods. *International Journal for Numerical Methods in Engineering*, 65:2167–2202, 2006.

Chen J. and Wang D. A constrained reproducing kernel particle formulation for shear deformable shell in cartesian coordinates. *International Journal for Numerical Methods in Engineering*, 68:151–172, 2006.

Ciarlet P.G. *Mathematical elasticity, Vol III: theory of shells*. North-Holland, 2000.

Cirak F. and Ortiz M. Fully C^1-conforming subdivision elements for finite deformation thin-shell analysis. *International Journal for Numerical Methods in Engineering*, 51(7):813–833, 2001.

Cirak F., Ortiz M., and Schröder P. Subdivision surfaces: a new paradigm for thin-shell finite-element analysis. *International Journal for Numerical Methods in Engineering*, 47:2039–2072, 2000.

Cyron C., Arroyo M., and Ortiz M. Smooth, second order, non-negative meshfree approximants selected by maximum entropy. *International Journal for Numerical Methods in Engineering*, 79(13):1605–1632, 2009.

do Carmo M.P. *Differential geometry of curves and surfaces*. Prentice-Hall, 1976.

Hoppe H., DeRose T., Duchamp T., McDonald J., and Stuetzle W. Surface reconstruction from unorganized points. In *SIGGRAPH '92: Proceedings of the 19th annual conference on Computer graphics and interactive techniques*, pages 71–78. ACM, New York, NY, USA,

1992. ISBN 0-89791-479-1.

Krysl P. and Belytschko T. Analysis of thin shells by the element-free Galerkin method. *International Journal of Solids and Structures*, 33(20-22):3057–3078, 1996.

Levin D. The approximation power of moving least-squares. *Mathematics of Computation*, 67(224):1517–1531, 1998. ISSN 0025-5718.

Levin D. Mesh-independent surface interpolation. In H. Brunnett and Mueller, editors, *Geometric Modeling for Scientific Visualization*, pages 37–49. Springer-Verlag, 2003.

Levoy M. and Whitted T. The use of points as displays primitives. Technical Report TR-85-022, Computer Science Department, University of North Carolina at Chappel Hill, 1985.

Millan D., Rosolen A., and Arroyo M. Nonlinear manifold learning for meshfree thin shell analysis. 2010a. In preparation.

Millan D., Rosolen A., and Arroyo M. Thin shell analysis from scattered points with maximum-entropy approximants. *International Journal for Numerical Methods in Engineering*, 2010b. doi:10.1002/nme.2992.

Noguchi H., Kawashima T., and Miyamura T. Element free analyses of shell and spatial structures. *International Journal for Numerical Methods in Engineering*, 47(6):1215–1240, 2000.

Ohtake Y., Belyaev A., Alexa M., Turk G., and Seidel H. Multi-level partition of unity implicits. *ACM Transactions on Graphics (Proc. SIGGRAPH 2003)*, 22:463–470, 2003.

Pauly M. *Point primitives for interactive modeling and processing of 3D geometry*. Ph.D. thesis, Federal Institute of Technology (ETH) of Zurich, 2003.

Rabczuk T., Areias P., and Belytschko T. A meshfree thin shell method for non-linear dynamic fracture. *International Journal for Numerical Methods in Engineering*, 72:525–548, 2007.

Simo J. and Fox D. On a stress resultant geometrically exact shell model. Part I: Formulation and optimal parametrization. *Computer Methods in Applied Mechanics and Engineering*, 72:267–304, 1989.

Simo J., Fox D., and Rifai M. On a stress resultant geometrically exact shell model. Part II: the linear theory; computational aspects. *Computer Methods in Applied Mechanics and Engineering*, 73:53–92, 1989.

Vaziri A. and Mahadevan L. Localized and extended deformations of elastic shells. 105(23):7913–7918, 2008. doi:10.1073/pnas.0707364105.

Zhang Z. and Wang J. Mlle: Modified locally linear embedding using multiple weights. In B. Schölkopf, J. Platt, and T. Hoffman, editors, *Advances in Neural Information Processing Systems 19*, pages 1593–1600. MIT Press, Cambridge, MA, 2007.